SCIENCE CHINA
Life Sciences

•RESEARCH PAPER•

July 2023 Vol.66 No.7: 1647–1664
https://doi.org/10.1007/s11427-022-2286-0

TaMADS29 interacts with TaNF-YB1 to synergistically regulate early grain development in bread wheat

Guoyu Liu†, Runqi Zhang†, Sen Li, Rehmat Ullah, Fengping Yang, Zihao Wang, Weilong Guo, Mingshan You, Baoyun Li, Chaojie Xie, Liangsheng Wang, Jie Liu, Zhongfu Ni, Qixin Sun & Rongqi Liang*

Frontiers Science Center for Molecular Design Breeding (MOE), State Key Laboratory for Agrobiotechnology, State Key Laboratory of Plant Physiology and Biochemistry, Key Laboratory of Crop Heterosis and Utilization (MOE), and Beijing Key Laboratory of Crop Genetic Improvement, China Agricultural University, Beijing 100193, China

Received November 5, 2022; accepted January 18, 2023; published online February 17, 2023

Grain development is a crucial determinant of yield and quality in bread wheat (*Triticum aestivum* L.). However, the regulatory mechanisms underlying wheat grain development remain elusive. Here we report how TaMADS29 interacts with TaNF-YB1 to synergistically regulate early grain development in bread wheat. The *tamads29* mutants generated by CRISPR/Cas9 exhibited severe grain filling deficiency, coupled with excessive accumulation of reactive oxygen species (ROS) and abnormal programmed cell death that occurred in early developing grains, while overexpression of *TaMADS29* increased grain width and 1,000-kernel weight. Further analysis revealed that TaMADS29 interacted directly with TaNF-YB1; null mutation in *TaNF-YB1* caused grain developmental deficiency similar to *tamads29* mutants. The regulatory complex composed of TaMADS29 and TaNF-YB1 exercises its possible function that inhibits the excessive accumulation of ROS by regulating the genes involved in chloroplast development and photosynthesis in early developing wheat grains and prevents nucellar projection degradation and endosperm cell death, facilitating transportation of nutrients into the endosperm and wholly filling of developing grains. Collectively, our work not only discloses the molecular mechanism of MADS-box and NF-Y TFs in facilitating bread wheat grain development, but also indicates that caryopsis chloroplast might be a central regulator of grain development rather than merely a photosynthesis organelle. More importantly, our work offers an innovative way to breed high-yield wheat cultivars by controlling the ROS level in developing grains.

chloroplast, grain filling, reactive oxygen species, TaMADS29, TaNF-YB1, wheat (*Triticum aestivum* L.)

Citation: Liu, G., Zhang, R., Li, S., Ullah, R., Yang, F., Wang, Z., Guo, W., You, M., Li, B., Xie, C., et al. (2023). TaMADS29 interacts with TaNF-YB1 to synergistically regulate early grain development in bread wheat. Sci China Life Sci 66, 1647–1664. https://doi.org/10.1007/s11427-022-2286-0

INTRODUCTION

Bread wheat (*Triticum aestivum* L.) is a pivotal staple food crop, providing about 20% of calories consumed by humans; therefore, it is vital to ensure a high and stable yield of wheat (Brenchley et al., 2012; Xiao et al., 2022). In bread wheat, the process of grain development initiates with double fertilization (Hehenberger et al., 2012). Following this, most of the nucellus degenerates, and the remaining tissue forms nucellar projection, which functions as a transfer tissue, delivering nutrients from the mother plant to the endosperm (Domínguez et al., 2001; Shewry et al., 2012). The grain development process can be divided into three phases: grain formation, grain filling, and grain maturity. Grain formation lasts for about 10 days and determines the grain storage capacity and grain length (Shewry et al., 2012). Subse-

†Contributed equally to this work
*Corresponding author (email: liangrq@cau.edu.cn)

quently, a large amount of the storage starch and proteins are accumulated in endosperm during grain filling, which directly determines grain width and grain weight, and eventually, wheat yield and quality (Kaushik et al., 2020). Accounting for about 70% of grain dry weight, starch is a major component of the wheat endosperm (McMaugh et al., 2014). As the precursor of its synthesis, sucrose is produced in source tissue (such as leaves) and transported into sink tissue (endosperm) via sugar transporters (SWEET, SUT), which is then converted into UDP-glucose and fructose (Chen et al., 2012; Koch, 2004). These substrates are then utilized by a series of enzymes, including ADP-glucose pyrophosphorylase (AGPase), granule bound starch synthase (Waxy), starch synthase (SS), starch branching enzyme, and starch debranching enzyme to catalyze the starch biosynthesis (McMaugh et al., 2014).

Programmed cell death (PCD) is a genetically regulated process that is precisely regulated by living organisms (Petrov et al., 2015). In plants, PCD plays a critical role in multiple growth and developmental processes, including grain development. For example, the wheat nucellar projection and endosperm undergo PCD during the middle and late stage of the crucial event of grain development (13–25 days after flowering (DAF)) (Domínguez et al., 2001; Li et al., 2018). PCD in plants could be triggered by the production of reactive oxygen species (ROS), including hydrogen peroxide (H_2O_2), singlet oxygen, and superoxide (Petrov et al., 2015; Ray et al., 2012). In higher plants, the chloroplast is one of the main sources of ROS production (Hu et al., 2021). In rice and *Arabidopsis*, it has been confirmed that high levels of ROS are associated with chloroplast dysfunction (Alamdari et al., 2021; Li et al., 2020; Rao et al., 2021; Ren et al., 2022). The ROS production is primarily catalyzed by NADPH oxidases and detoxified by the antioxidant enzymes, including peroxidase (POD), superoxide dismutase (SOD), ascorbate peroxidase (APX), and catalase (CAT) (Hu et al., 2017). As the key signaling component, ROS facilitates plant growth and tissue formation (Nestler et al., 2014). However, higher levels of ROS inevitably trigger oxidative damage, and even cell apoptosis and necrosis, which are detrimental to plant tissue development (Liu et al., 2016b). In rice, the ROS burst accompanied by endosperm PCD is delayed due to the elimination of excess ROS, suggesting that the onset of endosperm cell death might be induced by ROS (Wu et al., 2022; Xu et al., 2010). A previous study has demonstrated that *ZmSKS13* regulates maize grain development predominantly through the modulation of ROS homeostasis, suggesting that, in plant cells, a balance between ROS production and ROS scavenging is essentially required (Zhang et al., 2021). However, the functionality of ROS in regulating wheat development, especially wheat grain filling, is still undetermined.

A few transcription factors (TFs) contributing to grain filling have been characterized in different crop species, including *OsNF-YB1* and *OsPIL15* in rice (Bai et al., 2016; Ji et al., 2019), *O11* and *ZmABI19* in maize (Feng et al., 2018; Yang et al., 2021), and *TaRSR1*, *TabZIP28*, and *TaNAC019* in wheat (Gao et al., 2021; Liu et al., 2016a; Liu et al., 2020; Song et al., 2020). MADS-box genes, playing central roles in manipulating plant reproductive development, also contribute to grain development. In rice, *OsMADS78* and *OsMADS79* have been reported to control seed size and shape (Paul et al., 2020). To date, 201 MIKC-type MADS-box genes have been identified in Chinese Spring (Schilling et al., 2020), but their functions in wheat grain development remain largely unknown.

Here we report a dynamic transcriptional activation protein module, TaMADS29-TaNF-YB1. It is defined for inhibition of ROS accumulation via regulating chloroplast development and photosynthesis and preventing nucellar projection degradation and endosperm cell death, thereby maintaining nutrient transportation in early developing grains. These findings provide new insights into the molecular mechanism of MADS-box and NF-YB TFs in facilitating bread wheat seed development, and more importantly, may contribute to the genetic improvement of high-yield wheat breeding.

RESULTS

TaMADS29 is specifically expressed in early developing grains

To identify TF genes that are potentially involved in the control of grain development in wheat, we analyzed the dynamic transcriptome landscape of wheat grains at 4, 7, 10, 13, 16, 19, and 22 DAF, with total five starch synthesis-related enzyme genes, *TaAGPL1*, *TaGBSSI*, *TaSBEIIa*, *TaSSI*, and *TaSSII* being the "guide genes" to define the co-expressing genes. If two genes (the target gene and one of the "guide gene") result in an absolute value of the Pearson correlation coefficient greater than 0.8 between their expression profiles, they were considered coexpressing genes. In total, ninety-six TF genes belonging to MIKC_MADS, WRKY, ERF, bZIP, B3, AP2, and MYB families were identified (Figure S1A in Supporting Information). Notably, the MADS-box transcription factor 29 belonging to the MIKC_MADS family was highly expressed during the early and middle stages of wheat grain development, while its transcript levels in vegetative tissues, such as roots, stems, and leaves, were negligible (Figure 1A; Figure S1B in Supporting Information), suggesting its pivotal role in early and middle wheat grain development. Therefore, comprehensive research was conducted on wheat MADS-box transcription factor 29, hereafter designated as *TaMADS29*. Its three homologs were then named *TaMADS29-6A*, *TaMADS29-6B*, and *TaMADS29-6D* (International Wheat

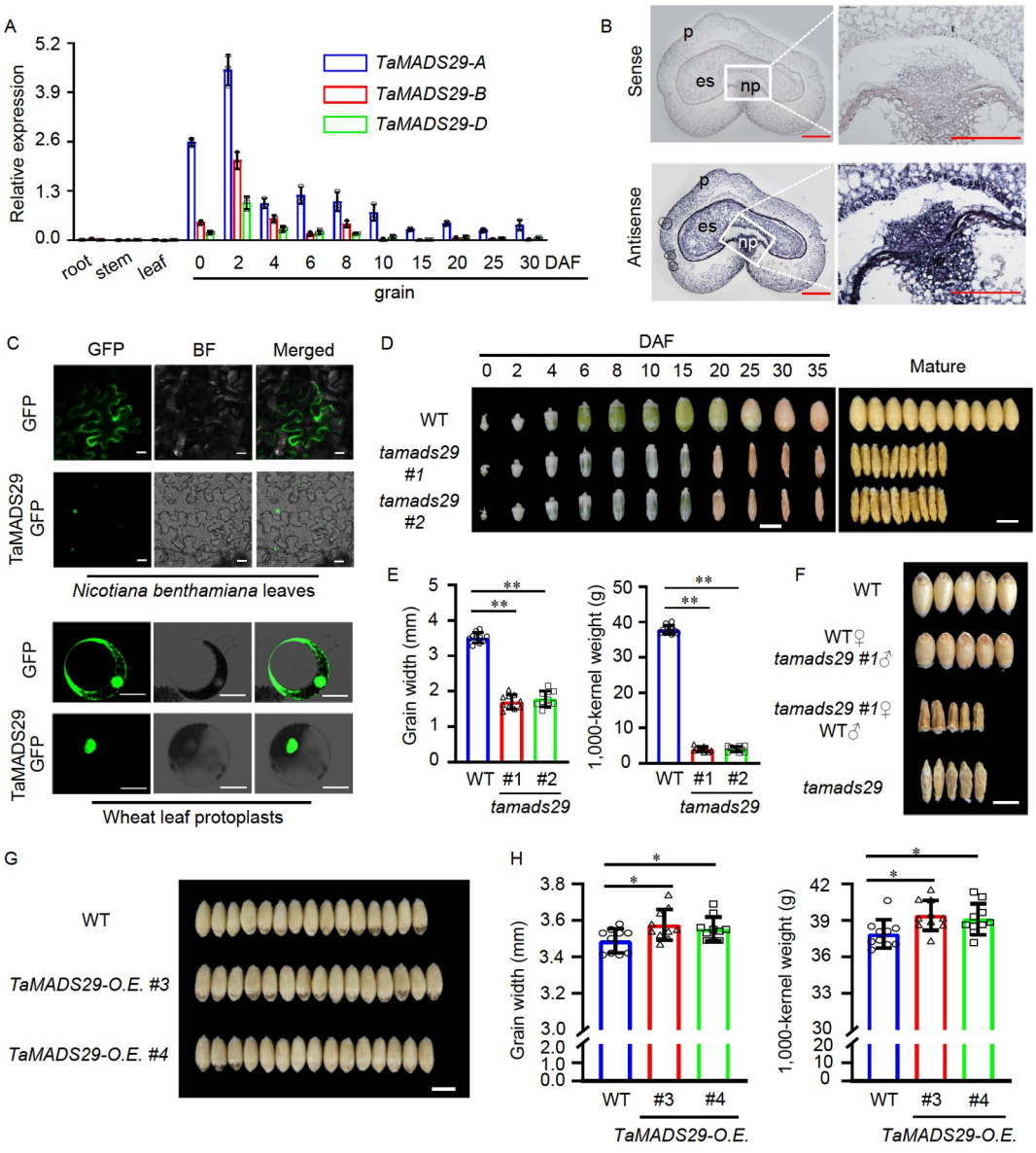

Figure 1 Expression pattern of *TaMADS29* and phenotypic analyses of *TaMADS29* transgenic lines. A, RT-qPCR analysis of the three *TaMADS29* homologous in various wheat tissues (root, stem, leaf) and grains from different developmental stages (0, 2, 4, 6, 8, 10, 15, 20, 25, and 30 DAF), as indicated by days after flowering. The wheat *Actin* gene was used as an internal control. Values are represented as mean±SD from three independent biological replicates. B, mRNA *in situ* hybridization of *TaMADS29* at 6 DAF grains. White boxes on the left side represent nucellar projection, which is magnified and represented on the right side. p, pericarp; es, endosperm; np, nucellar projection. For the left panel, bars=500 μm; right panel, bars=100 μm. C, Subcellular localization of *TaMADS29* in *Nicotiana benthamiana* leaves and wheat leaf protoplasts. Bars=20 μm. D, Developing grains and mature seeds of WT and *tamads29* mutants. Bars=5 mm. E, Difference of grain width and 1,000-kernel weight between WT and *tamads29* mutant lines. F, Mature seeds from reciprocal crosses between *tamads29 #1* and WT Fielder. Shrunken hybrid seeds were generated when WT pollen was used to pollinate *tamads29 #1*, while full seeds were generated when *tamads29 #1* pollen was employed to pollinate WT. Bar=5 mm. G, Mature seeds of WT and *TaMADS29* overexpression lines. Bars=5 mm. H, Comparative result of WT and *TaMADS29* overexpression lines on the basis of grain width and 1,000-kernel weight measurements. Data in E and H are represented as mean±SD (n=10), and P values were determined using Student's t-test. **, P<0.01; *, P<0.05.

Genome Sequencing Consortium, Appels et al., 2018), which share high sequence similarities (98.82%) and encode MADS-box TF proteins with 252, 253, and 252 amino acids (aa) in length, respectively (Figure S1C and D in Supporting Information).

Although the three *TaMADS29* homologs show quite similar expression patterns, their expression levels were contrastingly distinct, i.e., A>B>D, illustrating the expression asymmetry among the subgenomes (Figure 1A). The expression of *TaMADS29* in grain tissues was further evaluated utilizing RNA *in situ* hybridization. Results indicated that the *TaMADS29* transcripts were highly accumulated in the seed coat, endosperm, and nucellar projection at the early developmental stages of wheat grain (Figure 1B). To investigate the subcellular localization of TaMADS29 protein, a TaMADS29-GFP fusion was transiently expressed in wild

tobacco (*Nicotiana benthamiana*) leaves and wheat (Fielder) protoplast. Compared with the free GFP fluorescence, TaMADS29-GFP fusion protein fluorescence was only concentrated in the nucleus of tobacco leaves and wheat protoplast cells (Figure 1C), consistent with its function as a TF. Together, the above findings suggest that *TaMADS29* was specifically expressed in early developing grains, and its coding protein, as a nuclear-localized TF, may play important roles in wheat caryopsis development.

TaMADS29 positively regulates wheat grain development

To further explore the *in vivo* biological significance of *TaMADS29* in regulating wheat grain development, we generated *TaMADS29*-knockout (KO) mutant lines by CRISPR/Cas9 strategy engaging the spring wheat cultivar "Fielder" as the genetic background (Figure S2A in Supporting Information). Fifteen independent mutant lines were obtained. Among them, two lines harbor simultaneous frameshift mutations in all three *TaMADS29* homologs (*tamads29-abd* triple mutants, #1 and #2), thus were designated as *tamads29* mutants for further analysis. The *tamads29* mutants exhibit no obvious abnormality in plant height, spike length, and spikelet number per spike (Figure S2B–D in Supporting Information). In contrast, strong grain phenotypes were observed at various developmental stages after fertilization, consistent with the fact that *TaMADS29* was mainly expressed in developing grains. Before 4 DAF, no obvious difference was found in grain shape and size by comparing *tamads29* mutant lines with the wild-type (WT) Fielder. However, after 6 DAF, the *tamads29* mutants demonstrated a largely retarded grain growth rate compared to WT, resulting in extremely thin and shrunken mature seeds in *tamads29* mutants until 35 DAF, potentially due to the defect in dry matter accumulation (Figure 1D). Although no significant difference was found in grain length (GL) between *tamads29* and WT, the grain width (GW) and 1,000-kernel weight (TKW) in *tamads29* were dramatically reduced in comparison to the wild type (Figure 1E; Figure S2D in Supporting Information). Notably, single (*tamads29-a*, *tamads29-b*, and *tamads29-d*) and double (*tamads29-ab*, *tamads29-bd*, and *tamads29-ad*) mutations in *TaMADS29* homologs also led to significantly reduced TKW, but with a less severe phenotype in grain shape, suggesting the functional redundancy among *TaMADS29* homeologs and their dosage effect in regulating grain development (Figure S3 in Supporting Information). Interestingly, the phenotype (full or shrunken) of hybrid seeds from the crosses between *tamads29* and WT depends on the female parent, indicating that the defective seeds were due to the maternal defect (Figure 1F).

TaMADS29-overexpressing (myc-tagged) transgenic lines (*TaMADS29-O.E.*, #3 and #4) were also generated by using Fielder. The overexpression of *TaMADS29* and the accumulation of generated TaMADS29-Myc proteins in these transgenic lines were separately confirmed by qRT-PCR and immunoblotting assays (Figure S4A and B in Supporting Information). As shown in Figure 1G and 1H, as well as Figure S4C–G in Supporting Information, *TaMADS29-O.E.* lines and WT were similar in plant height, spike length, spikelet number per spike, and GL, while *TaMADS29-O.E.* lines exhibited higher GW (by 1.9%–2.5%) and TKW (by 3.2%–4%) in comparison to that of control plants, suggesting a positive regulatory role of *TaMADS29* in facilitating wheat grain development.

Loss of *TaMADS29* leads to an overaccumulation of ROS and earlier degradation of nucellar projection, and a blocked nutrient transportation into early developing wheat grains

Wheat caryopsis initiates PCD during grain development. As a result, only the embryo and aleurone layer remain alive in the mature seeds (Domínguez et al., 2001). Based on our observations, the grains from *tamads29* mutants exhibited early senescence and maturation (Figure 1D), suggesting an altered PCD pattern. To test this hypothesis, we performed trypan blue staining to detect cell death. The results showed that the trypan blue staining was very faint in both WT and *tamads29* mutant grains at 2 and 4 DAF (Figure S5A in Supporting Information). However, obviously elevated cell death in *tamads29* grains relative to that in WT at 6 DAF and beyond (Figure 2A; Figure S5A in Supporting Information). PCD was further examined using a terminal deoxynucleotidyl transferase dUTP nick-end labeling (TUNEL) assay. In WT grains, weak TUNEL signals could be detected only in the pericarp tissues, suggesting a mild cell death. However, considerably stronger TUNEL signals were spread all over the grain cross-section from *tamads29* mutants, including pericarp, endosperm, and nucellar projection (Figure 2B; Figure S5B in Supporting Information). In addition, the nucellar projection of *tamads29* grains collapsed, and cell layers significantly declined, suggesting that the nucellar projection cells of *tamads29* degraded (Figure 2C and D). Together, these observations support that *TaMADS29* is required for the transportation of nutrients, and a dramatically accelerated PCD is presented in wheat grains upon the loss of *TaMADS29*.

The ROS levels in 2, 4, and 6 DAF grains were determined by 2′,7′-dichlorodihydrofluorescein diacetate (H_2DCF-DA). The results showed that *tamads29* grains exhibited stronger fluorescence (approximately 2 fold higher, 6 DAF) than those in WT at 4 and 6 DAF, and the elevated ROS level seems to be earlier than the cell death in *tamads29* grains (Figure 2E and F; Figure S5A in Supporting Information). Furthermore, H_2O_2 content was determined in both 6 DAF

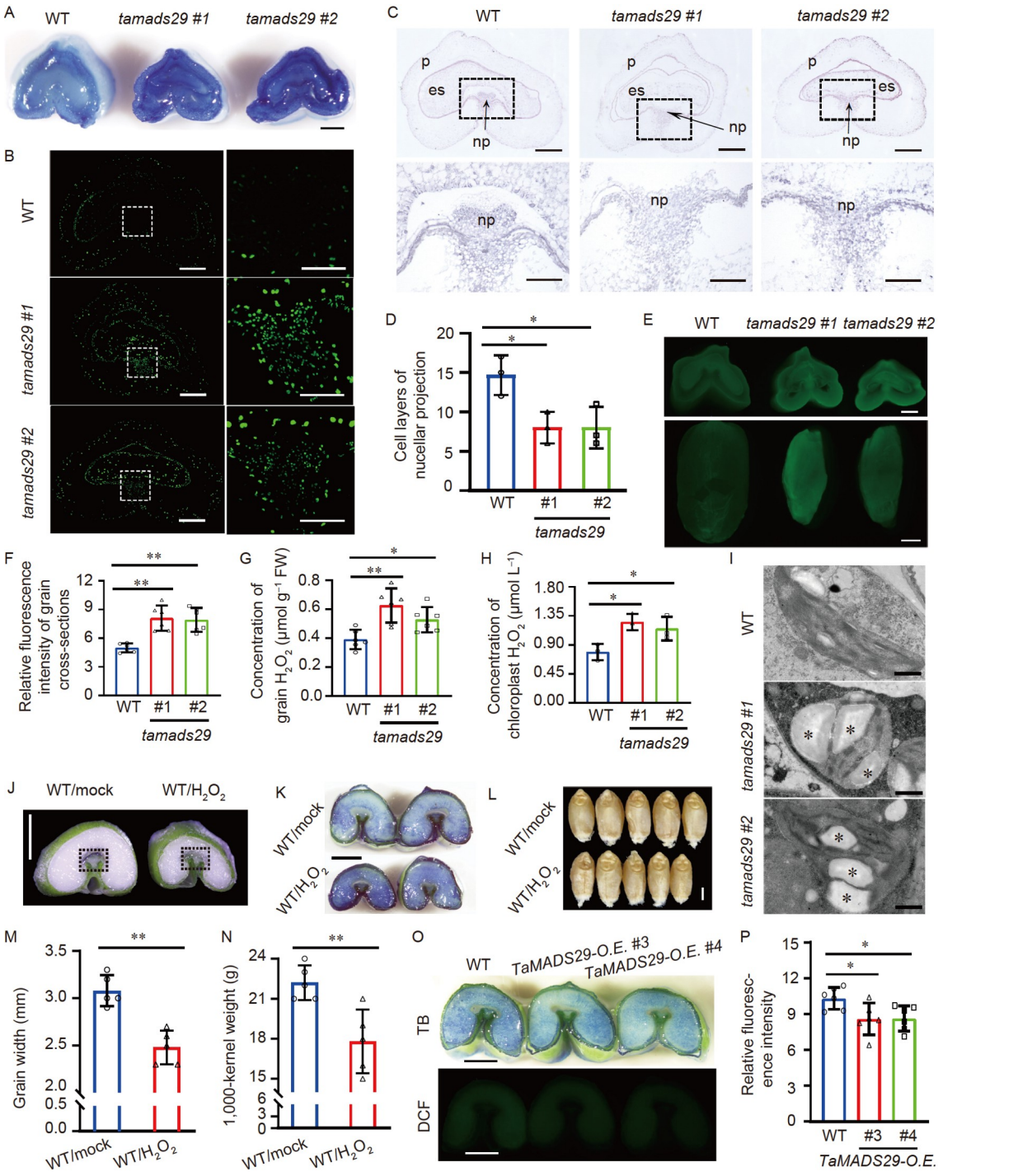

Figure 2 Loss of *TaMADS29* led to the overaccumulation of ROS and abnormal PCD in developing wheat grains. A, TB staining of the 6 DAF grains from WT and *tamads29* mutants. Bar=500 μm. B, TUNEL analysis of 6 DAF grains from WT and *tamads29* mutants. White boxes in the left panel were magnified and represented in the right panel. For the left panel, bars=500 μm; right panel, bars=200 μm. C, Transverse section of 6 DAF grains revealed the nucellar projection degradation in the *tamads29* mutants. Black boxes in the top panel were magnified and represented in the lower panel. p, pericarp; es, endosperm; np, nucellar projection. For the top panel, bars=500 μm; lower panel, bars=200 μm. D, Quantification of cell layers in the nucellar projection of 6 DAF grains from WT and *tamads29* mutants. n=3. E, DCF staining of the 6 DAF grains from WT and *tamads29* mutants. Note: the grain pericarp has been removed in the lower panel. Bars=500 μm. F, Quantification of DCF fluorescence intensities shown in E. n=6. G and H, Concentration of H_2O_2 in 6 DAF grains (G, n=6) and chloroplasts from these grains (H, n=3) in WT and *tamads29* mutants. I, TEM observation of chloroplasts in 6 DAF grains from WT and *tamads29* mutants. Bars=1 μm. J, Exogenous ROS (1 mol L^{-1} H_2O_2, treated for 10 d) repressed grain filling and reduced nucellar projection. Bar=2 mm. K, TB staining of wheat grains in J. Bar=2 mm. L, Mature grains that were treated with exogenous ROS for 10 d or untreated (Mock). Bar=2 mm. M and N, Difference of grain width and 1,000-kernel weight shown in L. n=5. O, TB and DCF staining using 15 DAF grains from WT and *TaMADS29* overexpression lines. Bars=2 mm. P, Quantification of DCF fluorescence intensities shown in O. n=6. Data in D, F, G, H, M, N and P are represented as mean±SD, and P values were determined using Student's t-test. **, P<0.01; *, P<0.05.

grains and caryopsis chloroplast by spectrophotometry. The result was consistent with total ROS levels—*tamads29* grains accumulated significantly higher levels of H_2O_2 than the WT, with an even higher concentration in the caryopsis chloroplast (Figure 2G and H). Under TEM, chloroplasts of WT grains demonstrated a well-structured internal membrane system with well-organized thylakoids and several small starch granules. However, in *tamads29* grains, chloroplasts were swelled by more and larger starch granules, resulting in disordered thylakoids (Figure 2I). This is consistent with the previous report that overaccumulation of ROS is associated with developmental defects in the chloroplast (Alamdari et al., 2021; Hu et al., 2021; Li et al., 2020; Rao et al., 2021; Ren et al., 2022).

To further validate the effects of ROS on nucellar projection, we tried to mimic the *tamads29* phenotype by spraying H_2O_2 on early developing WT grains. After exogenous H_2O_2 treatment for 10 days, the reduced nucellar projection (Figure 2J) with deeper stained by trypan blue (Figure 2K), the GW and grain weight were significantly reduced in the WT Fielder (Figure 2L–N; Figure S6 in Supporting Information), which strongly supported that the ROS H_2O_2 is a key regulator of nucellar projection degradation.

Contrary to the above observations, the wheat grains from *TaMADS29-O.E.* lines exhibited lighter TB staining and weaker DCF fluorescence than those in WT at 15 DAF, demonstrating the reduced ROS level and delayed PCD process in *TaMADS29-O.E.* lines (Figure 2O and P). Together, these findings suggest a key role of *TaMADS29* in conditioning the fate of nucellar projection and endosperm in wheat grains.

The nucellar projection functions as a transfer tissue to distribute nutrients (mainly in the form of sucrose) from the mother plant to the endosperm (Chen et al., 2012; Domínguez et al., 2001; Shewry et al., 2012). Consistent with the degradation of nucellar projection in *tamads29* mutants, a significant reduction of sucrose content was detected in 6 DAF grains of *tamads29* in comparison to WT (Figure 3A). Correspondingly, the sucrose contents in flag leaves of *tamads29* were significantly increased (Figure 3B). Next, the grain phenotypes of *tamads29* (6 DAF and mature kernels) were further analyzed in detail by conducting microscopic observation. Unlike WT, the grain cross-section of *tamads29* was shaped irregularly and exhibited smaller endosperm, thicker pericarp, and diminished endosperm cells (Figure 3C and D). Moreover, in *tamads29* mutants, large amounts of starch granules were accumulated in the pericarp of the early developing grains, while few or relatively smaller starch granules were detected in the endosperm (Figure 3C). Further observations in mature grains also confirmed that the formation of normal starch granules was completely deficient in *tamads29* mutants (Figure 3E).

In summary, these findings imply the essential role of *TaMADS29* in maintaining grain filling and repressing the overaccumulation of ROS.

TaMADS29 directly regulates the expression of genes involved in chloroplast development and photosynthesis in wheat grain

To further dissect the potential molecular basis underlying the effect of *TaMADS29* in regulating wheat kernel development, transcriptome analyses were performed using the 2, 4, and 6 DAF grains collected from *tamads29* and WT. The results showed that 1,251, 3,566, and 9,718 DEGs in 2, 4, and 6 DAF grains, respectively (Figure S7A and Table S1 in Supporting Information). Among these DEGs, 427 genes were defined as overlapping DEGs in all the tested developmental stages, indicating their fundamental roles in early wheat grain development (Figure S7B in Supporting Information). In addition, consistent with the inadequacy in starch accumulation (Figure 3E), the transcripts of some sugar transporter genes and starch synthesis related genes were drastically decreased in *tamads29* developing grains (especially at 6 DAF) relative to that in WT (Figure S7C and Table S2 in Supporting Information). To validate the transcriptome results, the expression of these genes was further validated by qRT-PCR (Figure S7D in Supporting Information).

Gene ontology (GO) analysis revealed multiple biological processes, molecular functions, and cellular components were enriched in the DEGs, including “cellular response to reactive oxygen species,” “response to oxidative stress,” “nutrient reservoir activity,” “chlorophyll synthetase activity,” “isoamylase complex,” “chloroplast,” “photosystem I,” and “photosystem II” (Figure 4A; Table S3 in Supporting Information). Specifically, the signaling pathways relating to endosperm development, regulation of ROS metabolic process, pullulanase activity, and amyloplast were enriched by the down-regulated DEGs, whereas pathways associating with the regulation of H_2O_2 biosynthetic process, chloroplast organization, chloroplast relocation, chlorophyll binding, and chloroplast envelope were exclusively enriched by the up-regulated genes (Figure 4A; Table S3 in Supporting Information). Interestingly, chlorophyll catabolic process and chlorophyllase activity were enriched by down-regulated genes at 2 and 4 DAF, while they were enriched by up-regulated genes at 6 DAF (Figure 4A; Table S3 in Supporting Information). Together, these data suggest that *TaMADS29* maintains wheat grain development through the modulation of chloroplast development and photosynthesis and ROS metabolic process.

When ROS level is elevated in plants, the transcript levels of ROS scavenging related genes will be enhanced by the antioxidant system (Mittler, 2017). As described in Figure 2G and H, overaccumulation of ROS was detected in

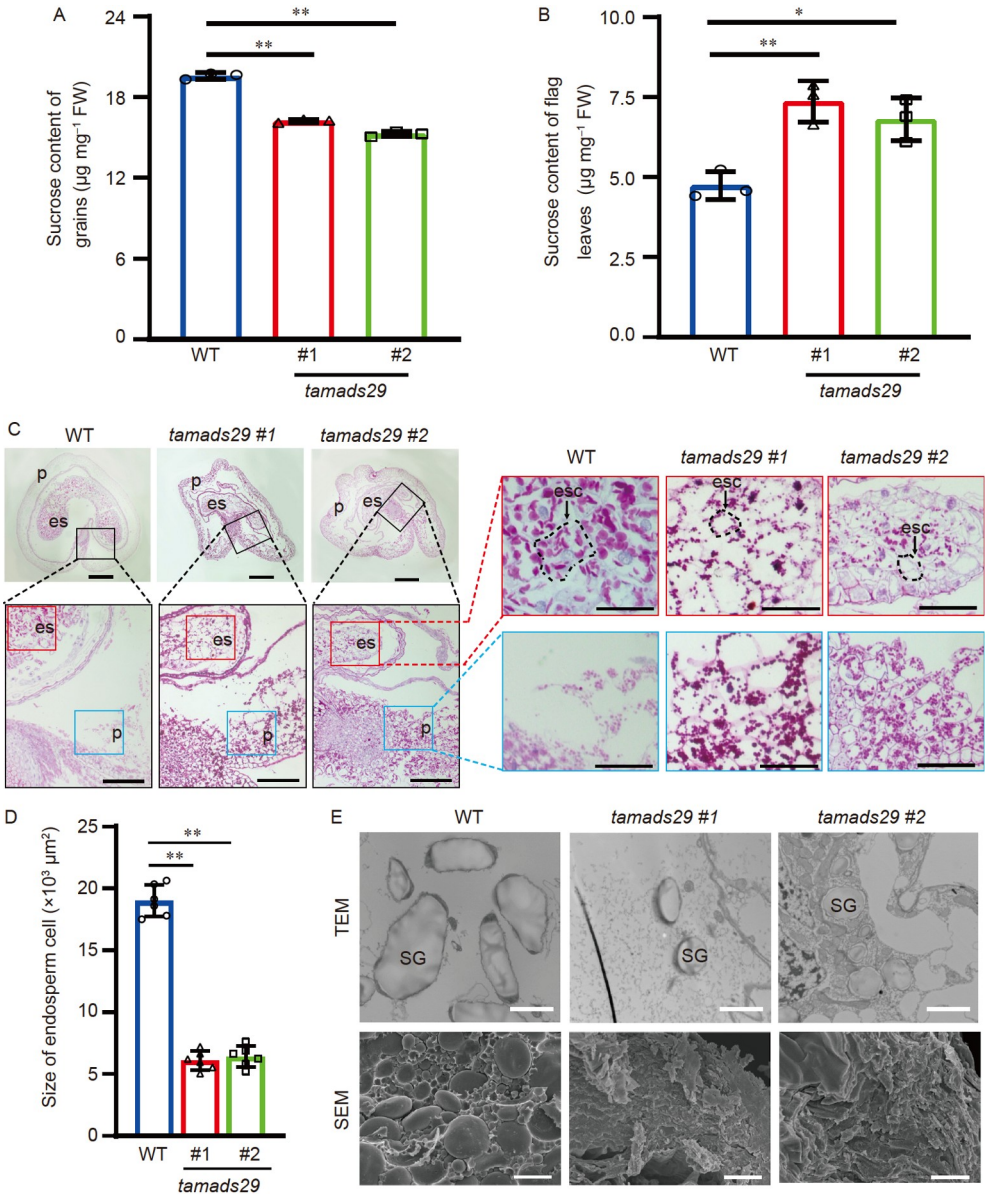

Figure 3 Null mutation in *TaMADS29* repressed the nutrient transportation and starch biosynthesis in early developing wheat grains. A and B, Sucrose content of 6 DAF grains (A) and flag leaves (B) from WT and *tamads29* mutants. FW, fresh weight. *n*=3. C, Median transverse sections of 6 DAF grains from WT and *tamads29* mutants. Magnified images were represented in black, red, and blue boxes, respectively. p, pericarp; es, endosperm; esc, endosperm cell. For the left panel, bars=500 μm; right panel, bars=200 μm. D, Difference of endosperm cell size in 6 DAF grains from WT and *tamads29* mutants. *n*=6. E, TEM (top panel) and SEM (low panel) observation of wheat endosperm from WT and *tamads29* mutants. 6 DAF and mature grains were utilized for TEM and SEM, respectively. SG, starch granules. For TEM, bars=2 μm; SEM, bars=20 μm. Data in A, B, and D are represented as mean±SD, and *P* values were determined using Student's *t*-test. **, $P<0.01$; *, $P<0.05$.

tamads29 mutant grains, presumably due to abnormal chloroplasts. In accordance with these results, our transcriptome data revealed that most of the genes involved in ROS scavenging, including *TaPOD*, *TaSOD*, *TaAPX*, and *TaCAT*, as well as genes encoding photosystem II protein, were upregulated in *tamads29* grains (Figure 4B; Tables S4 and S5 in Supporting Information), while most of the other genes involved in chloroplast development and photosynthesis, including *TaFtsH*, *TaCHUP1*, *TaFtsZ2-1*, and *TaYcf3*, were downregulated in *tamads29* grains (Figure 4C and D; Figure S8 and Table S6 in Supporting Information). Interestingly, high-confident MADS-box TF binding CArG-box cis-elements were detected in the promoter regions (2 kb) of most of these genes, suggesting that these genes may be the downstream targets of TaMADS29 (Figure 4C). Among them, the physical association of TaMADS29 with the probe that mimicked the CArG-box-containing *TaFtsH1* promoter sequence was confirmed by electrophoretic mobility shift assay (EMSA) and ChIP-qPCR (Figure 4E and F). Furthermore, we determined the effect of TaMADS29 on down-

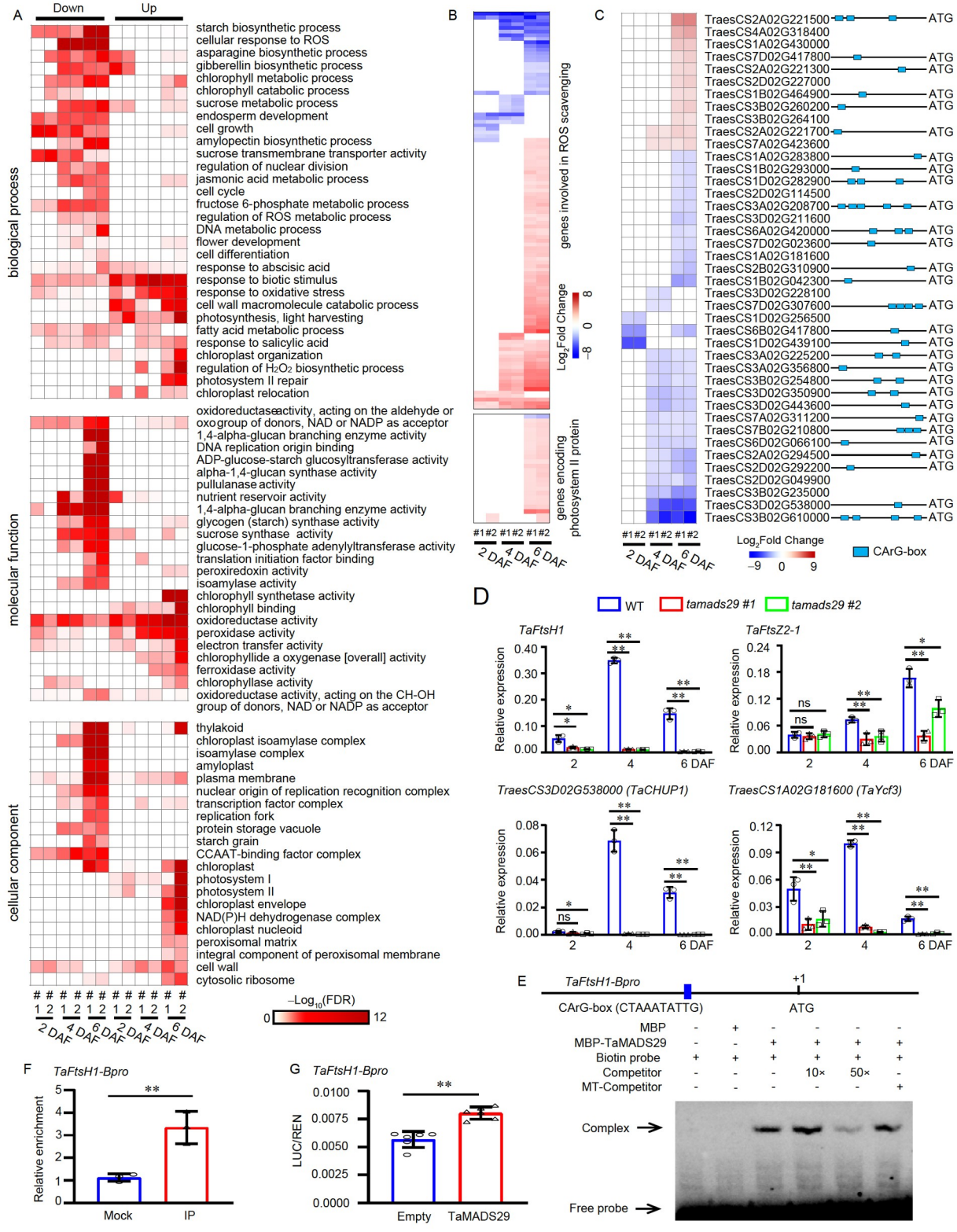

Figure 4 TaMADS29 regulated the expression of genes involved in chloroplast development and photosynthesis. A, GO terms exhibiting statistically significant enrichment in DEGs. #1 and #2 represent the line number of *tamads29* mutants. B, Heat-map revealing the fold changes of DEGs involved in ROS scavenging and encoding photosystem II protein in *tamads29* mutants in comparison to that in WT. C, Heat-map revealing the fold changes of DEGs involved in chloroplast development and photosynthesis in *tamads29* mutants in comparison to that in WT. D, RT-qPCR assay confirming the relative expression of *TaFtsH1*, *TaFtsZ2-1*, *TaCHUP1*, and *TaYcf3* in *tamads29* mutants and WT. n=3. E and F, EMSA assay (E) and ChIP-qPCR (F, n=3) showing the association of TaMADS29 with the CArG-box in the promoter of *TaFtsH1 in vitro* and *in vivo*, respectively. G, Dual-luciferase transcriptional activity (LUC/REN) of TaMADS29 with the promoter of *TaFtsH1*. n=6. Data in D, F, and G are represented as mean±SD, and P values were determined using Student's t-test. **,

stream gene expression. First, we generated *TaFtsH1*$_{pro}$*::LUC*/*35S::REN* (*TaFtsH1*$_{pro}$*::LUC*) as a reporter system, where the firefly luciferase (*LUC*) reporter gene was driven by the promoter of *TaFtsH1*, and the Renilla luciferase (*REN*) internal signal control gene was driven by the CaMV 35S promoter. Then, the effector *TaMADS29* was co-expressed with the *LUC*/*REN* reporters. As expected, the expression of *TaMADS29* indeed significantly enhanced the transcription of *TaFtsH1*, illustrated by the upregulated LUC/REN signals (Figure 4G).

To summarize, our findings indicated a key role of *TaMADS29* in the regulation of relevant ROS levels in wheat grains via, at least partly, the regulation of genes related to chloroplast development and photosynthesis in early developing wheat grains.

TaMADS29 interacts with nuclear factor Y subunit NF-YB for transcriptional activation activity

To understand the molecular basis conferring TaMADS29 transcriptional regulation activity, we identified TaMADS29-interacting proteins through the screening of the wheat grain-derived yeast two-hybrid (Y2H) cDNA library. As a result, 35 proteins were identified to potentially interact with TaMADS29 (Table S7 in Supporting Information). Among these candidates, the nuclear factor Y subunit NF-YB was of particular interest because its transcript level was also down-regulated in the 4 and 6 DAF grains of *tamads29* (Figure S9A in Supporting Information), and the coding gene of TaNF-YB1 is also highly expressed in the early and mid-developing grains (Figure S9B in Supporting Information), implying its genetic interaction with *TaMADS29*, as well as its involvements in grain development. In addition, the subcellular localization results indicated that the TaNF-YB1 protein is located in both the cytoplasm and nucleus (Figure S9C in Supporting Information). Therefore, we carried out firefly luciferase complementation imaging (LCI), bimolecular fluorescent complementation (BiFC), and the *in vivo* co-immunoprecipitation (Co-IP) assays, and confirmed the *in vivo* interactions between TaMADS29 and TaNF-YB1 (Figure 5A–D). Notably, the TaMADS29-TaNF-YB1 complexes were mainly concentrated in the nucleus of tobacco leaves (Figure 5C).

Next, we evaluated the potential roles of TaNF-YB1 on TaMADS29 transcriptional activation activity. We expressed *TaMADS29* and *TaNF-YB1* alone, respectively, and co-expressed *TaMADS29* with *TaNF-YB1 (TaMADS29*/*TaNF-YB1)* (Figure 5E) to test their effects in activating the *TaFtsH1*$_{pro}$*::LUC* reporters. Interestingly, significantly higher LUC/REN signals were observed in *TaMADS29*/*TaNF-YB1* co-expressing samples compared to those in *TaMADS29*- or *TaNF-YB1*-expressing ones (Figure 5E). Consistent with these observations, EMSA assays confirmed that TaNF-YB1 could indeed bind to CCAAT-box in the promoter region of *TaFtsH1* (Figure 5F). In addition, TaMADS29 binds to both the CCAAT-box and CArG-box, while TaNF-YB1 binds only to the CCAAT-box in the promoter of *TaFtsH1* (Figure S9D and E in Supporting Information). Together, these findings confirm the additive effects between TaMADS29 and TaNF-YB1 in activating gene expression and suggest the possibility that these two TFs act synergistically to initiate downstream signals *in vivo*.

Genetic validation of *TaNF-YB1* function in grain development

The above results demonstrated that the TaNF-YB1 factor may define a key regulatory hub in conditioning TaMADS29 function and, consequently, grain filling. To test this hypothesis, we generated the *TaNF-YB1*-KO mutant lines, *tanf-yb1*, through CRISPR/Cas9 strategy in the Fielder genetic background (Figure S10A in Supporting Information). Similar to that of *tamads29*, the two *tanf-yb1* lines (#5 and #6), with the three *TaNF-YB1* homoeologous genes being simultaneously knocked out, also showed partial deficiency in grain filling, represented by the slight depression that appeared on the dorsal side of the caryopsis at 15 DAF (also visible at 10 DAF through cross-sectional observation), smaller and shrink mature kernels, and significantly reduced GL, GW, TKW, and grain starch content (Figure 6A–E; Figures S10B–D and S11 in Supporting Information). Meanwhile, the grain development-related genes that displayed attenuated expression levels in *tamads29* grains, including *TaFtsH1*, *TaSWEET11*, *TaSUS2*, *TaAGPL1*, *TaGBSSI*, and *TaSSI*, also exhibited extremely reduced transcript levels in the 15 DAF grains of *tanf-yb1* (Figure 6F; Figure S12 in Supporting Information). In addition, after staining with trypan blue and H_2DCF-DA, *tanf-yb1* grains exhibited deeper blue staining signals and stronger fluorescence, especially in the nucellar projection (Figure 6G and H), suggesting the elevated PCD and ROS levels in *tanf-yb1* grains. These findings support the notion that TaMADS29 and TaNF-YB1 are interdependently required for grain filling.

DISCUSSION

MADS-box TFs are essential for various processes during the plant reproductive stage, such as floral determinacy and seed development, in several crops, including maize, barley, and rice (Shoesmith et al., 2021; Wu et al., 2019; Yin and Xue, 2012). Our results illustrated that the loss of function of *TaMADS29* severely attenuated wheat grain development and the accumulation of storage substance, leading to retarded grain growth rate and starch biosynthesis deficiency (Figures 1D and 3C–E; Figure S7C and D in Supporting

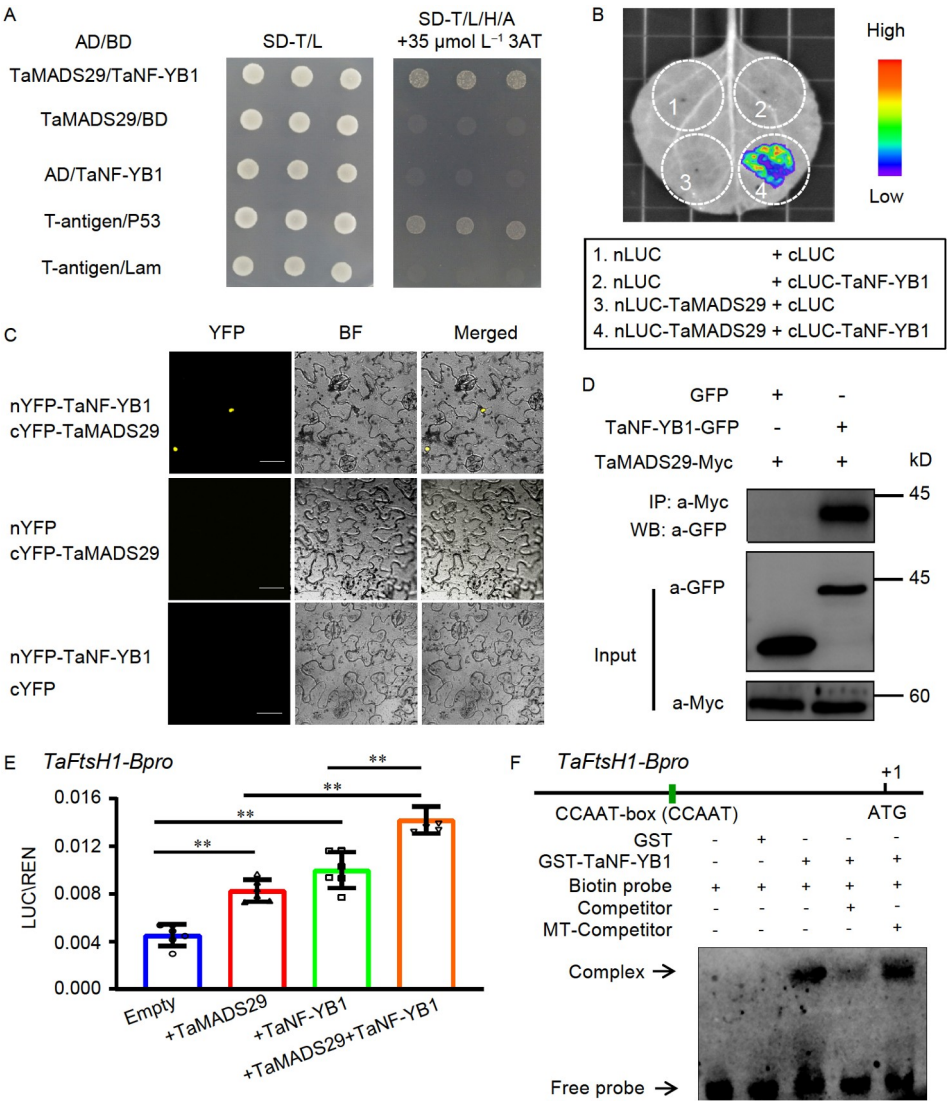

Figure 5 TaMADS29 interacted with TaNF-YB1 to cumulatively activate the expression of *TaFtsH1*. A–D, The interaction of TaMADS29 with TaNF-YB1 were confirmed by Y2H (A), LCI (B), BiFC (C) and Co-IP (D), respectively. BF, bright field. Bars=20 μm. E, Dual-luciferase transcriptional activity (LUC/REN) of different effectors (TaMADS29, TaNF-YB1, and TaMADS29/TaNF-YB1) with the promoter of *TaFtsH1*. Data are represented as mean±SD (n=6), and P values were determined using Student's t-test. **, P<0.01. F, EMSA assay showing that TaNF-YB1 binds to CCAAT-box in the promoter of *TaFtsH1 in vitro*.

Information). In contrast, overexpression of *TaMADS29* significantly increased GW and TKW, confirming the positive modulatory roles of *TaMADS29* in wheat grain development (Figure 1G and H). Previous studies in other crop species have revealed a similar function of MADS29 in grain development. For example, loss-of-function of *OsMADS29* in rice represses grain filling and consequently results in shriveled and/or aborted seeds (Nayar et al., 2013; Yang et al., 2012; Yin and Xue, 2012); similar grain developmental deficiency was also observed in *HvMADS29*-KO barley mutants (Shoesmith et al., 2021). These findings suggest the highly conserved roles of *MADS29* in regulating grain development in different cereal crop plants.

In higher plants, the embryo and endosperm (filial seed organs) develop within maternal tissues, including nucellus, nucellar projection, inner and outer integuments, and pericarp (Radchuk et al., 2011). Among them, nucellar projection functions as the nutrient source for filial tissues and undergoes PCD during cereal grain development (Domínguez et al., 2001; Yin and Xue, 2012). In rice, the PCD process coupled with cell degradation in nucellar projection is initiated in early developing grains (3 DAF), which is required for the development of rice grain (Yin and Xue, 2012). Previous studies revealed that the PCD-related genes in rice grains were directly stimulated by *OsMADS29*. Knocking down of this gene repressed the PCD process and cell degradation in nucellar projection, thus preventing the transportation of nutrients and resulting in shrunken seeds (Yang et al., 2012; Yin and Xue, 2012). Unlike that of rice, the PCD process in wheat nucellar projection and en-

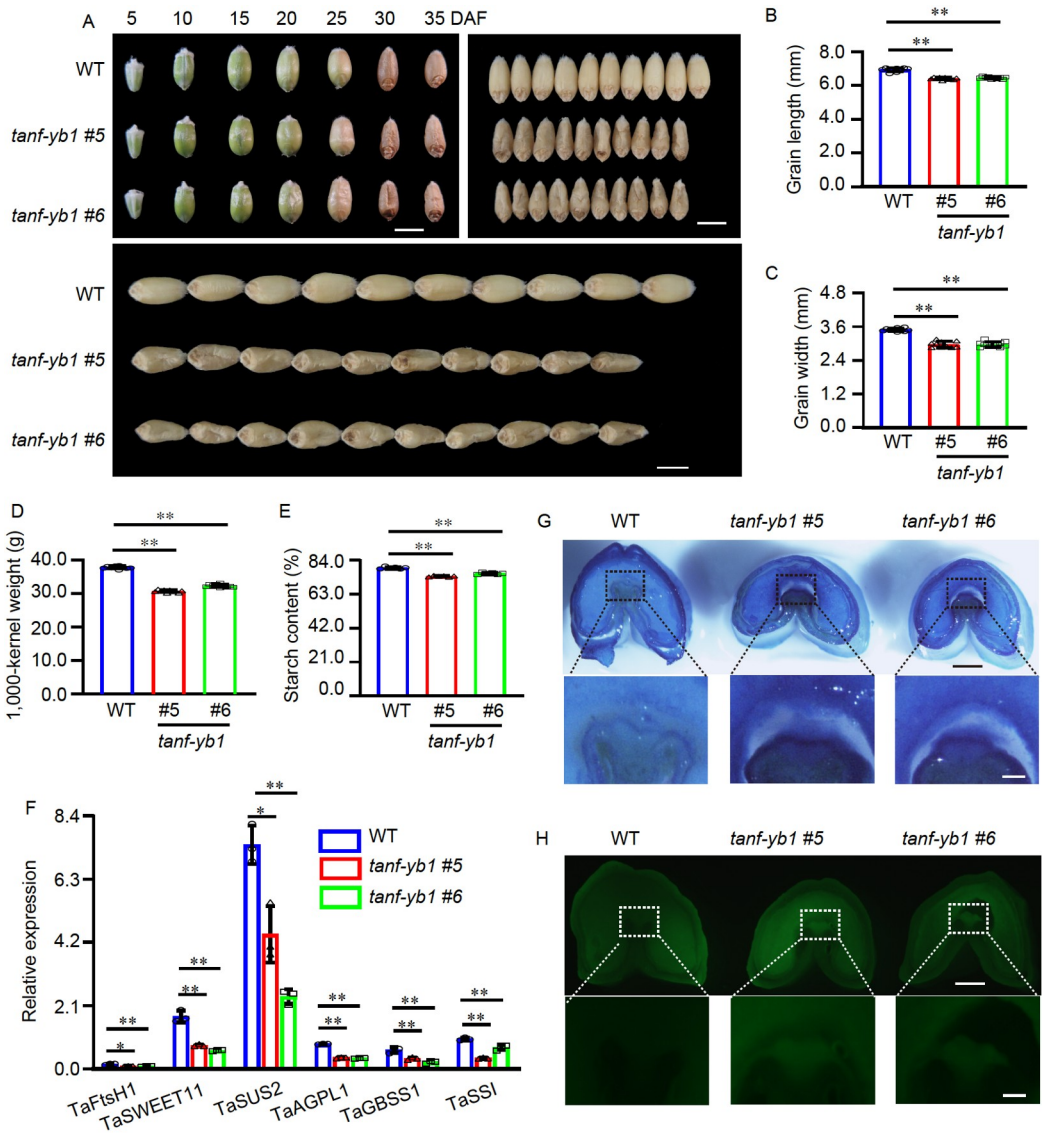

Figure 6 Phenotypes of wheat *tanf-yb1* knockout mutants. A, Developing grains and mature seeds of WT and *tanf-yb1* mutants. Bar=5 mm. B–E, Comparative analysis of grain length (B), grain width (C), 1,000-kernel weight (D), and starch content (E) between WT and *tanf-yb1* mutant lines. *n*=10. F, Transcriptional level of genes involved in chloroplast development and photosynthesis, sugar transport and starch biosynthesis in WT and *tanf-yb1* grains at 15 DAF. *n*=3. G–H, TB (G) and DCF (H) staining using 15 DAF grains from WT and *tanf-yb1* mutants. Black or white boxes in the top panel were magnified and represented in the lower panel. For the top panel, bars=500 μm; lower panel, bars=100 μm. Data in B–F are represented as mean±SD, and *P* values were determined using Student's *t*-test. **, $P<0.01$; *, $P<0.05$.

dosperm cells initiates at 13 and 25 DAF, respectively, demonstrating that the PCD process in nucellar projection is not required in early developing wheat grains (Domínguez et al., 2001; Li et al., 2018). In this study, different phenotypes of hybrid seeds from reciprocal crosses implied the defects in the maternal tissue of the *tamads29* mutant (Figure 1F). Consistent with this, wheat *tamads29* mutant grain exhibited strong PCD response not only in the endosperm but also in nucellar projection, coupled with cell collapse (Figure 2A–D). Given the decreased sucrose content in wheat grains and the increased sucrose content in photosynthetic organs (flag leaves), we speculated that the degradation of nucellar projection blocked the nutrient transportation between mother plants and filial organs in early developing wheat grains, leading to shrunken seeds (Figure 3A and B). Further analysis revealed the dramatically upregulated ROS levels in *tamads29* grains (Figure 2E–G), and similar phenotype (reduced nucellar projection with decreased grain size and grain weight) could be induced by exogenous ROS in WT Fielder (Figure 2J–N; Figure S6 in Supporting Information). In contrast, the ROS level was significantly decreased in *TaMADS29 O.E.* lines, coupled with the delayed PCD process (Figure 2O and P). These results demonstrated that although the functional inhibition of MADS29 displayed a similar phenotype in rice and wheat, the molecular bases underlying the MADS29-

regulated grain development are largely divergent.

MADS-box transcription factors have been shown to play key roles in the biogenesis of chloroplasts (Wang et al., 2019), one of the main sources of ROS production in plants (Hu et al., 2021). Previous studies indicated that over-accumulation of ROS is associated with developmental defects in chloroplast and triggers PCD (Alamdari et al., 2021; Hu et al., 2021; Li et al., 2020; Rao et al., 2021; Ren et al., 2022). In addition to leaves, most of the developing caryopsis of grasses, including wheat, barley, and rice, are photosynthetically active in seed coats. It has been reported that chloroplasts in developing caryopsis not only produce sufficient ATP and NADPH to meet local energy demand but also supply oxygen to sustain respiratory energy for storage activity and nutrient transport within the endosperm (Radchuk and Borisjuk, 2014). As a highly versatile signal, ROS has been demonstrated to induce various stress responses. For example, the release of ROS singlet oxygen ($^1O_2$) triggers cell death in seedlings and inhibits mature plant growth in *Arabidopsis fluorescent (flu)* mutant (Wang et al., 2020). Some important proteins, including filamentation-temperature-sensitive protein H (FtsH), chloroplast unusual positioning protein (CHUP), hypothetical chloroplast open reading frame (YCF) protein, protein filamenting temperature-sensitive Z (FtsZ), translocon of the outer membranes of chloroplasts (TOC), and outer envelope pore protein, are related to the chloroplast development and photosynthesis (Andrès et al., 2010; Barth et al., 2022; Kato and Sakamoto, 2018; Nellaepalli et al., 2018; Porter et al., 2021; Usami et al., 2012). Among them, ATP-dependent zinc metalloprotease FtsH is encoded by *TaFtsH*, whose transcription is directly activated by TaMADS29 (Figure 4E–G). A lack of FtsH led to the generation of high levels of ROS (Kato et al., 2009; Kato and Sakamoto, 2018). In this study, significantly increased H_2O_2 content and abnormal structures of chloroplast were detected in *tamads29* grains (Figure 2H and I). Meanwhile, the transcriptome analysis demonstrated that multiple signaling pathways relating to chloroplast and ROS were enriched by the DEGs between *tamads29* mutants and WT (Figure 4A). In addition, EMSA, ChIP-qPCR, and transcriptional activation activity assays confirmed the important role of TaMADS29 in the transcriptional regulation of genes involved in chloroplast development and photosynthesis (Figure 4 E–G). In summary, we inferred that null mutation of TaMADS29 repressed the expression of genes involved in chloroplast development and photosynthesis, led to defects in the chloroplast and caused overaccumulation of ROS and earlier degradation of nucellar projection and endosperm cells, thereby blocking the nutrient transportation into endosperm and generating the shrunken seeds.

In this study, reduced nucellar projection with decreased grain size and grain weight could be induced by exogenous H_2O_2 in WT Fielder; meanwhile, the increased ROS level and delayed PCD process in *TaMADS29-O.E.* lines further revealed the relationship between ROS and PCD. Although ROS produced by chloroplasts in *tamads29* mutants is accompanied by degraded nucellar projection and endosperm cell death, whether it is the direct cause of PCD remains to be further determined. On the other hand, the PCD process is accompanied by ROS burst; the elevated ROS may be an effect of more dying cells. For example, ROS was triggered in rice during the salt stress-induced early stage of PCD (Chen et al., 2009). Accumulation of ROS, such as H_2O_2, can not only trigger but also facilitate stress and PCD-associated pathways (Cui et al., 2013; Desikan et al., 1998; Mittler et al., 2004). Therefore, the large amount of ROS in the *tamads29* mutant was related to the regulation of cell death in nucellar projection and endosperm, and their causal relationship needs further study.

Different TFs may interact with each other to synergistically regulate the common downstream target genes. For example, *OsPDCD5* negatively regulates salt tolerance, plant architecture, and yield in rice, and these pleiotropic effects were at least partially achieved through its direct interaction with *OsAGAP* (Dong et al., 2021). In our study, TaMADS29 directly interacts with TaNF-YB1 (Figure 5). Specially, in tobacco leaves, the TaMADS29-TaNF-YB1 complexes were mainly located in the nucleus (Figure 5C), whereas the TaNF-YB1 protein was located in both cytoplasm and nucleus (Figure S9C in Supporting Information). These results suggest that TaMADS29 assists TaNF-YB1 in the cytoplasm to enter the nucleus or retains bound TaNF-YB1 in the nucleus to additively regulate the downstream signaling pathway. In rice, OsNF-YB1 activate *SUT1*, *SUT3*, and *SUT4* through direct binding to the CCAAT boxes in their promoter region; knockout of OsNF-YB1 led to the defective grain filling with reduced starch granules in size (Bai et al., 2016). Similarly, EMSA assays confirmed that TaNF-YB1 activates the expression of *TaFtsH1* via direct association with the CCAAT-box in their promoter regions (Figure 5F). Interestingly, according to the previous study, the sequence of the CCAAT-box is part of the sequence of the CArG-box (de Folter and Angenent, 2006); thus, TaMADS29 binds to both the CCAAT-box and CArG-box. Therefore, TaMADS29 and TaNF-YB1 share the common binding site as these two TFs have a concurrent positive impact on the expression of *TaFtsH1*. Meanwhile, the mature seeds of the *tanf-yb1* mutant also displayed grain filling deficiency similar to that of *tamads29* mutants (Figure 6A–E). Further observation exhibited the evidently augmented PCD and aggravated ROS level in the *tanf-yb1* mutant grains (Figure 6G and H). More importantly, TaNF-YB1 could significantly enhance the transcriptional activation activity of TaMADS29. These findings suggest the additive effects among TaMADS29 and TaNF-YB1 in manipulating the downstream signaling transduction (Figure 5E). Although

both *tamads29* and *tanf-yb1* mutants exhibited grain developmental deficiency, the loss of function of *TaMADS29* resulted in substantially more rigorous grain development deficiency than that of *tanf-yb1* mutants. Regarding the cause of this phenomenon, we infer that the first is the *TaMADS29* peak expressed earlier than *TaNF-YB1*; thus, its regulation in grain development is more dominant. Meanwhile, sequences of CArG-box are more diverse; therefore, potentially additional genes could be regulated by TaMADS29 in comparison to TaNF-YB1. Furthermore, the transcriptional level of *TaNF-YB1* was significantly downregulated in *tamads29* mutant grains, which indicated that the function of *TaNF-YB1* has also been affected in *tamads29* mutant, suggesting that the phenotype of *tamads29* mutant may be partly contributed by transcriptional inhibition of *TaNF-YB1*.

In summary, we assume that TaMADS29 interacts with TaNF-YB1 to form a transcriptional activation protein complex, which at least partly regulates the chloroplast development and photosynthesis via direct association with the promoter region of related genes, thus inhibiting the overaccumulation of ROS and preventing cell death of endosperm and nucellar projection (Figure 7). Our results support a theoretical basis for the investigation of early wheat grain development and, more importantly, provide new insights into the function of chloroplast in developing caryopsis and the molecular mechanism of MADS-box and NF-Y TFs in facilitating cereal grain development.

Grain development and filling remarkably determine the grain weight and final wheat grain yield formation (Bednarek et al., 2012). As an important component of wheat yield, grain weight has high heritability and therefore is a key breeding target to boost wheat yield (Kuchel et al., 2007). Both ectopic overexpression and genome editing technologies can be employed for the improvement of agronomic traits in modern high-yield molecular breeding (Lu et al., 2014; Luo et al., 2021). In the present study, a significant increase of TKW was observed after the overexpression of *TaMADS29* (Figure 1G and H), implying the potential value of this gene in modern wheat molecular breeding. Accordingly, the manipulation of *TaMADS29* through overexpression or transgenic approaches may facilitate the development of new wheat varieties with high yield potential.

MATERIALS AND METHODS

Plant materials

Wheat plants were grown in an isolated experimental field at China Agricultural University, Beijing (E116°, N40°) and in a greenhouse at 26°C/20°C and 75% relative humidity under a 16-h light and 8-h dark photoperiod. For co-expression analysis, 4, 7, 10, 13, 16, 19, and 22 DAF grains were col-

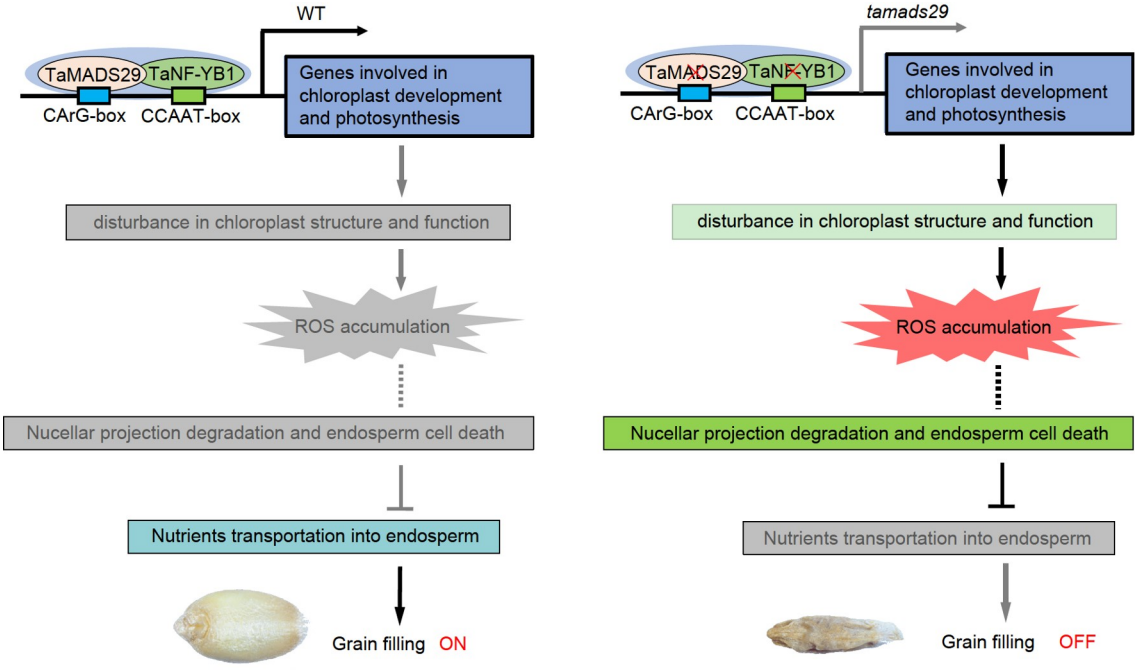

Figure 7 Proposed working model of *TaMADS29* modulating wheat grain development. *TaMADS29* interacts with TaNF-YB1 to form a transcriptional activation protein complex, which directly regulates the transcription of genes involved in chloroplast development and photosynthesis, ensures the normal structure and function of chloroplast, inhibits the overaccumulation of ROS, prevents cell death of endosperm and nucellar projection, maintains the transportation of nutrients into endosperm, and allows the normal grain filling. Blunt (⊥) and sharp arrows (→) represent inhibition and promotion effects, respectively; the unfunctional pathway is shown in gray.

lected from plants grown in the field. Root, stem, leaf, and developing grains were harvested for gene expression analysis. Tissue samples were collected from three individual plants for each developmental stage. All samples were immediately frozen in liquid nitrogen and then stored at −80°C.

RNA-seq and data analysis

RNA-seq libraries were prepared with Poly-A Purification TruSeq library reagents and sequenced on Illumina HiSeqTM 2500 platform (Illumina, USA). After screening and trimming, the remaining reads were mapped to the wheat reference genome sequence IWGSCv1.1. The Bioconductor package DESeq2 was used to perform DEG analysis with an absolute value of P value<0.05 and $|\mathrm{Log_2}$ (Fold Change)|>1. GO enrichment analysis was performed using Triticeae-Gene Tribe (http://wheat.cau.edu.cn/TGT/m5/?navbar=-GOEnrichment) (Chen et al., 2020).

Quantitative qRT-PCR and protein analysis

Total RNA was extracted from wheat developing grains and vegetative tissues using an RNAprep Pure Plant Kit (Tiangen, Beijing, China) and RNAprep Pure Plant Kit (Tiangen), respectively. cDNA was synthesized using a reverse transcription kit (TaKaRa, Japan). Quantitative Real-time PCR was performed on the 7500 Real-Time PCR System (Applied Biosystems, USA) with SYBR Premix Ex Taq (TaKaRa). Relative quantification of gene expression was calculated using the $2^{-\Delta Ct}$ method, in which the wheat *Actin* (GenBank accession No. AB181991) gene was used as an internal control. All analyses were repeated at least three times. Primers used for qRT-PCR are listed in Table S8 in Supporting Information. Total proteins were extracted from developing grains (6 DAF) of *TaMADS29-O.E.* lines or WT and were analyzed by employing the western blot experiment with an anti-Myc antibody (TransGen Biotech, Beijing, China).

mRNA *in situ* hybridization

Fresh wheat grains (6 DAF) were fixed in 4% paraformaldehyde, following dehydration, then the fixed wheat grains were embedded in paraffin (Sigma-Aldrich, USA), sectioned at 8 μm using a microtome (Leica, Germany). The 247 bp conserved sequence of *TaMADS29* three homologous cDNA was amplified and used as a template to prepare sense and antisense RNA probes using a DIG RNA labeling kit (Roche, USA). The hybridization and the detection of hybridized signals were performed as described previously (Jiang et al., 2019). The primers used are listed in Table S8 in Supporting Information.

Subcellular localization

The open reading frame (ORF) of *TaMADS29-6A* and *TaNF-YB1-6D* without a termination codon were cloned into the *Xba*I site of the pCAMBIA1300-CaMV35S-GFP vector to produce the fusion constructs. Relevant primer sequences are listed in Table S8 in Supporting Information. The GFP fusion constructs and GFP control were transformed into young leaves of 4-week-old *Nicotiana benthamiana* leaves using *Agrobacterium tumefaciens* (strain GV3101) infiltration. The transformed tobacco plants were cultured at 24°C for 48 h. In addition, the above GFP fusion constructs and GFP control plasmid were also transferred into wheat protoplasts. Wheat protoplasts were incubated at 28°C for 18 h in the dark. GFP fluorescence signal was monitored by LSM880 confocal laser scanning microscope (Carl Zeiss, Germany).

Generation of constructs and transformation

Two sgRNAs target sequences of *TaMADS29* and *TaNF-YB1* were designed using the E-CRISPR design website (http://www.e-crisp.org/E-CRISP/designcrispr.html). After amplification with two pairs of primers (Table S8 in Supporting Information), the sgRNAs were cloned into the *pBUE411* vector. The CRISPR-Cas9 constructs were transformed into wheat cultivars Fielder using *Agrobacterium tumefaciens*-mediated (strain EHA105) transformation (Ishida et al., 2015). To generate the overexpression construct, the ORF of *TaMADS29-6A* from Fielder and the Myc domain sequences were amplified and linked by PCR, then the *TaMADS29-Myc* fragment was inserted into the pMWB122 vector and transformed into wheat cultivar Fielder using *Agrobacterium*-mediated (strain EHA105) transformation (Ishida et al., 2015).

ROS detection and measurement of H_2O_2 content

ROS detections were conducted by H_2DCF-DA staining as described previously (Wu et al., 2022). To detect the cell viability, wheat grains were also performed trypan blue staining according to previous literature (Wang et al., 2020). Each sample was photographed with a stereo microscope (Nikon Digital Sight DS-Fi2, Japan).

Chloroplasts of wheat grains (6 DAF from *tamads29* mutants) were isolated using a plant seed active chloroplast iso kit (GENMED, GMS16007.2, USA). H_2O_2 content of 6 DAF grains and chloroplasts from these grains were detected utilizing the Amplex Red Hydrogen Peroxide/Peroxidase Assay kit (Invitrogen, USA). Six independent measurements were performed for the analysis.

TUNEL assay

Wheat grains from *tamads29* mutants and WT were collected

at 6 DAF. TUNEL assay was performed using a TUNEL apoptosis detection kit (DeadEnd Fluorometric TUNEL system, Promega, USA). TUNEL signals were observed using a confocal laser fluorescence microscope (Carl Zeiss).

Histological analysis

Immature wild-type and *tamads29* mutant seeds at 6 DAF were collected. Seeds were fixed in FAA (50% ethanol, 5% glacial acetic acid, and 5% formaldehyde) for 24 h at room temperature. The paraffin sections assay was performed as reported previously (Gao et al., 2021) and stained with Periodic Acid Schiff, then observed with a light microscope (Motic, Beijing, China).

TEM and SEM assay

For TEM observation, the developing grains at 6 DAF of *tamads29* mutants and the WT were crosscut and fixed in 4% paraformaldehyde; the ultrathin sections were obtained as previously described (Li et al., 2018) and stained with uranyl acetate and alkaline lead citrate, then examined with a Talos L120C transmission electron microscope (Thermo Fisher Scientific, USA). For SEM observation, the mature grains of *tamads29* mutants and WT were cut transversely and gold-plated and then were observed with a scanning electron microscope (JSM-6390LV, Japan).

Treatment of WT kernels with exogenous ROS

After pollination, the glumes of WT spikes were cut with scissors, 1 mol L^{-1} H_2O_2 was evenly sprayed on the spikes, and the mock-treated controls were sprayed with sterilized water. After 10 d, the phenotypes of fresh grains under different treatment conditions were observed.

Quantification of sucrose content

The sucrose content of immature seeds and flag leaves from WT and *tamads29* mutants was measured using a sucrose/D-glucose/D-fructose content detection kit (Roche) according to the manufacturer's protocol. Total starch content was measured using a total starch assay kit (Megazyme, Ireland) according to the manufacturer's protocol.

EMSA

EMSA was performed as previously described with minor modifications (Pei et al., 2022). The CDS of *TaMADS29-6A* and *TaNF-YB1-6D* was cloned into the pMAL-C2 and pGEX6P-1 vector, respectively. These recombinant proteins were transferred into *E. coli* BL21 (DE3) (Weidi Biotechnology, Shanghai, China). Recombinant protein expression was induced with 0.1 mmol L^{-1} IPTG overnight at 16°C when A_{600} reached 0.6. The protein was purified using amylose resin (New England Biolabs, USA) and GST·bind™ resin (Millipore, USA), respectively. DNA probes containing CArG-box or CCAAT-box were synthesized and labeled with biotin at the 5′ end. Unlabeled probes which substituted for CArG-box or CCAAT-box and the original unlabeled probes were used as m-competitors and competitors, respectively. EMSA assays were performed using the Light Shift Chemiluminescent EMSA Kit (Thermo Fisher Scientific). The recombinant proteins and probes were mixed in the DNA binding reactions: 1×binding buffer (100 mmol L^{-1} Tris, 500 mmol L^{-1} KCl, 10 mmol L^{-1} DTT; pH 7.5), 2.5% glycerol, 0.2 mmol L^{-1} EDTA and 50 ng mL^{-1} poly [dI•dC]. The binding reactions were incubated at 25°C for 20 min, and then the mixture was loaded onto 6% (w/v) native polyacrylamide gels. The binding reactions were transferred to a nylon membrane (GE Healthcare, USA) and UV cross-linked. Biotin-labeled DNA was detected using the above kit, and signals were visualized using the Tanon-5200 image system (Tanon, Shanghai, China). The probes are shown in Table S8 in Supporting Information.

Chromatin immunoprecipitation-quantitative PCR

The ChIP assay was performed as previously described (Jiang et al., 2019). Wheat grains (10 DAF) of the *TaMADS29-Myc* transgenic lines were collected and cross-linked with 1% (v/v) formaldehyde in a vacuum desiccator for 10 min. The protein-DNA complex was immunoprecipitated with Magna ChIP™ Protein A+G Magnetic Beads (Merck Millipore, USA) and Anti-Myc (Abcam, UK). DNA precipitates were recovered by a QIAquick PCR purification kit (Qiagen, Germany) and were quantified by qRT-PCR. Equal amounts of seed tissues and ChIP purification products were used for each reaction. ChIP-qPCR primers are listed in Table S8 in Supporting Information.

Yeast two-hybrid

Wheat grains were sampled at 5, 10, 15, 20, and 25 DAF for cDNA library construction. The cDNA library was constructed at Shanghai Ouyi Biotech Company. For yeast two-hybrid screening, the full-length CDS of *TaMADS29* was cloned into the pGBKT7 vector and transformed into Y2HGold yeast cells for screening of the above yeast cDNA expression library. The pGBKT7-p53 and pGADT7-T were co-transformed into Y2HGold as positive controls, while pGBKT7-lam and pGADT7-T were used as negative controls. Full-length of *TaNF-YB1-6D* and *TaMADS29-6A* were fused into pGBKT7 and pGADT7 vectors, respectively. These combined plasmids were co-transformed into Y2HGold, which were grown on DDO (SD/-Leu/-Trp) plates

and QDO (SD/-Leu/-Trp/-Ade/-His) plates. The primers used are listed in Table S8 in Supporting Information.

Co-IP assay

The Co-IP assay was performed according to a previous publication (Liu et al., 2017). *TaMADS29-6A* and *TaNF-YB1-6D* were combined into pMWB122 and pCambia1300-GFP vectors to produce the Myc- and GFP-fused constructs and transformed into *Agrobacterium* strain GV3101. The *Agrobacterium* harboring different constructs of Myc and GFP vector pairs were transformed into *Nicotiana benthamiana* leaves. Total proteins were extracted using the lysis buffer (50 mmol L^{-1} Tris-HCl at pH 7.5, 150 mmol L^{-1} NaCl, 5 mmol L^{-1} EDTA at pH 8.0, 0.1% Triton X-100, 0.2% NP-40) with freshly added PMSF (phenylmethylsulphonyl fluoride, 10 mmol L^{-1}) and protease inhibitor cocktail (Roche). Anti-Myc- and Anti-GFP-tag mAb-Magnetic Agarose (MBL, Japan) were used for the immunoprecipitation. In western blotting, anti-Myc (TransGen Biotech) and anti-GFP (TransGen Biotech) antibodies were used for the detection of Myc- and GFP-tagged proteins, respectively. In total, three independent biological replicates were performed.

LCI assay

The full-length ORF of *TaNF-YB1-6D* was fused into linearized pCAMBIA1300-cLUC, the full-length ORF of *TaMADS29-6A* without a stop codon were cloned into linearized pCAMBIA1300-nLUC, respectively. These plasmids were transiently expressed in *Nicotiana benthamiana* leaves by *Agrobacterium*-mediated infiltration (strain GV3101). After 48 h, LUC activities were detected using NightSHADE LB 985 (Berthold Technologies, Germany).

BiFC assay

To construct TaMADS29-YFPC, the full-length ORF of *TaMADS29-6A* was cloned into linearized pSPYCE (M) vectors. Similarly, the full-length ORF of *TaNF-YB1-6D* without a stop codon was fused into linearized pSPYNE173 vectors, respectively. The combination of plasmids was co-expressed in 3–4-week-old *Nicotiana benthamiana* leaves using *Agrobacterium tumefaciens* (strain GV3101) infiltration. After 48 h, the YFP fluorescence signals were examined with a confocal laser fluorescence microscope (LSM880; Carl Zeiss). Three biological replications were performed with similar results.

Dual-luciferase transcriptional activity assay

Transient transcription dual-luciferase assays were carried out as previously described (Gao et al., 2021). About 2.0 kb promoter of *TaFtsH1* was cloned into the *pGreenII 0800-LUC* vector, respectively. The full CDS of *TaMADS29-6A* and *TaNF-YB1-6D* were cloned into the PHB vector as effectors. The reporter and effector constructs were separately introduced into *Agrobacterium* strain GV3101 to carry out co-infiltration in *Nicotiana benthamiana* leaves. LUC and REN activities were measured utilizing the Dual-Luciferase Reporter Assay System (Promega). Six independent measurements were performed for the analysis.

Data availability

Sequence data from this article are available at the EnsemblPlants website, http://plants.ensembl.org/index.html (TraesCS6A02G158100 (*TaMADS29-A*); TraesCS6B02G186700 (*TaMADS29-B*); TraesCS6D01G147400 (*TaMADS29-D*); TraesCS6A02G287500 (*TaNF-YB1-A*); TraesCS6B02G316800 (*TaNF-YB1-B*); TraesCS6D02G268200 (*TaNF-YB1-D*)). RNA-seq data were deposited in the NCBI with accession numbers PRJNA791126 and PRJNA790694. All other study data are included in the article and Supporting Information.

Compliance and ethics *The author(s) declare that they have no conflict of interest.*

Acknowledgements *This work was supported by the National Key Research and Development Program of China (2022YFF1002902, 2016YFD0100803). The authors are grateful to Dr.s Lubin Tan and Jinsheng Lai (China Agricultural University) for their helpful discussions and comments on the text. We thank Dr. Na Song (China Agricultural University) for helping with tissue culture and wheat transformation and Dr. Jian Chen (China Agricultural University) for suggestions about ChIP optimization.*

References

Alamdari, K., Fisher, K.E., Tano, D.W., Rai, S., Palos, K., Nelson, A.D.L., and Woodson, J.D. (2021). Chloroplast quality control pathways are dependent on plastid DNA synthesis and nucleotides provided by cytidine triphosphate synthase two. New Phytol 231, 1431–1448.

Andrès, C., Agne, B., and Kessler, F. (2010). The TOC complex: preprotein gateway to the chloroplast. Biochim Biophys Acta 1803, 715–723.

Appels, R., Eversole, K., Stein, N., Feuillet, C., Keller, B., Rogers, J., Pozniak, C.J., Choulet, F., Distelfeld, A., Poland, J., et al. (2018). Shifting the limits in wheat research and breeding using a fully annotated reference genome. Science 361, 7191.

Bai, A.N., Lu, X.D., Li, D.Q., Liu, J.X., and Liu, C.M. (2016). NF-YB1-regulated expression of sucrose transporters in aleurone facilitates sugar loading to rice endosperm. Cell Res 26, 384–388.

Barth, M.A., Soll, J., and Akbaş, Ş. (2022). Prokaryotic and eukaryotic traits support the biological role of the chloroplast outer envelope. Biochim Biophys Acta 1869, 119224.

Bednarek, J., Boulaflous, A., Girousse, C., Ravel, C., Tassy, C., Barret, P., Bouzidi, M.F., and Mouzeyar, S. (2012). Down-regulation of the *TaGW2* gene by RNA interference results in decreased grain size and weight in wheat. J Exp Bot 63, 5945–5955.

Brenchley, R., Spannagl, M., Pfeifer, M., Barker, G.L.A., D'Amore, R., Allen, A.M., McKenzie, N., Kramer, M., Kerhornou, A., Bolser, D., et

al. (2012). Analysis of the bread wheat genome using whole-genome shotgun sequencing. Nature 491, 705–710.
Chen, L.Q., Qu, X.Q., Hou, B.H., Sosso, D., Osorio, S., Fernie, A.R., and Frommer, W.B. (2012). Sucrose efflux mediated by SWEET proteins as a key step for phloem transport. Science 335, 207–211.
Chen, X., Wang, Y., Li, J., Jiang, A., Cheng, Y., and Zhang, W. (2009). Mitochondrial proteome during salt stress-induced programmed cell death in rice. Plant Physiol Biochem 47, 407–415.
Chen, Y., Song, W., Xie, X., Wang, Z., Guan, P., Peng, H., Jiao, Y., Ni, Z., Sun, Q., and Guo, W. (2020). A collinearity-incorporating homology inference strategy for connecting emerging assemblies in the Triticeae tribe as a pilot practice in the plant pangenomic era. Mol Plant 13, 1694–1708.
Cui, M.H., Ok, S.H., Yoo, K.S., Jung, K.W., Yoo, S.D., and Shin, J.S. (2013). An *Arabidopsis* cell growth defect factor-related protein, CRS, promotes plant senescence by increasing the production of hydrogen peroxide. Plant Cell Physiol 54, 155–167.
de Folter, S., and Angenent, G.C. (2006). *trans* meets *cis* in MADS science. Trends Plant Sci 11, 224–231.
Desikan, R., Reynolds, A., Hancock, T.J., and Neill, J.S. (1998). Harpin and hydrogen peroxide both initiate programmed cell death but have differential effects on defence gene expression in *Arabidopsis* suspension cultures. Biochem J 330, 115–120.
Domínguez, F., Moreno, J., and Cejudo, F.J. (2001). The nucellus degenerates by a process of programmed cell death during the early stages of wheat grain development. Planta 213, 352–360.
Dong, S., Dong, X., Han, X., Zhang, F., Zhu, Y., Xin, X., Wang, Y., Hu, Y., Yuan, D., Wang, J., et al. (2021). *OsPDCD5* negatively regulates plant architecture and grain yield in rice. Proc Natl Acad Sci USA 118, e2018799118.
Feng, F., Qi, W., Lv, Y., Yan, S., Xu, L., Yang, W., Yuan, Y., Chen, Y., Zhao, H., and Song, R. (2018). OPAQUE11 is a central hub of the regulatory network for maize endosperm development and nutrient metabolism. Plant Cell 30, 375–396.
Gao, Y., An, K., Guo, W., Chen, Y., Zhang, R., Zhang, X., Chang, S., Rossi, V., Jin, F., Cao, X., et al. (2021). The endosperm-specific transcription factor TaNAC019 regulates glutenin and starch accumulation and its elite allele improves wheat grain quality. Plant Cell 33, 603–622.
Hehenberger, E., Kradolfer, D., and Köhler, C. (2012). Endosperm cellularization defines an important developmental transition for embryo development. Development 139, 2031–2039.
Hu, H., Ren, D., Hu, J., Jiang, H., Chen, P., Zeng, D., Qian, Q., and Guo, L. (2021). *WHITE AND LESION-MIMIC LEAF1*, encoding a lumazine synthase, affects reactive oxygen species balance and chloroplast development in rice. Plant J 108, 1690–1703.
Hu, S., Yu, Y., Chen, Q., Mu, G., Shen, Z., and Zheng, L. (2017). *OsMYB45* plays an important role in rice resistance to cadmium stress. Plant Sci 264, 1–8.
Ishida, Y., Tsunashima, M., Hiei, Y., and Komari, T. (2015). Wheat (*Triticum aestivum* L.) transformation using immature embryos. In: Wang, K., ed. Agrobacterium Protocols. Methods in Molecular Biology. New York: Springer. 189–198.
Jiang, L., Ma, X., Zhao, S., Tang, Y., Liu, F., Gu, P., Fu, Y., Zhu, Z., Cai, H., Sun, C., et al. (2019). The APETALA2-Like transcription factor SUPERNUMERARY BRACT controls rice seed shattering and seed size. Plant Cell 31, 17–36.
Ji, X., Du, Y., Li, F., Sun, H., Zhang, J., Li, J., Peng, T., Xin, Z., and Zhao, Q. (2019). The basic helix-loop-helix transcription factor, OsPIL15, regulates grain size via directly targeting a purine permease gene *OsPUP7* in rice. Plant Biotechnol J 17, 1527–1537.
Kato, Y., Miura, E., Ido, K., Ifuku, K., and Sakamoto, W. (2009). The variegated mutants lacking chloroplastic FtsHs are defective in D1 degradation and accumulate reactive oxygen species. Plant Physiol 151, 1790–1801.
Kato, Y., and Sakamoto, W. (2018). FtsH protease in the thylakoid membrane: physiological functions and the regulation of protease activity. Front Plant Sci 9, 855.
Kaushik, M., Rai, S., Venkadesan, S., Sinha, S.K., Mohan, S., and Mandal, P.K. (2020). Transcriptome analysis reveals important candidate genes related to nutrient reservoir, carbohydrate metabolism, and defence proteins during grain development of hexaploid bread wheat and its diploid progenitors. Genes 11, 509.
Koch, K. (2004). Sucrose metabolism: regulatory mechanisms and pivotal roles in sugar sensing and plant development. Curr Opin Plant Biol 7, 235–246.
Kuchel, H., Williams, K.J., Langridge, P., Eagles, H.A., and Jefferies, S.P. (2007). Genetic dissection of grain yield in bread wheat. I. QTL analysis. Theor Appl Genet 115, 1029–1041.
Li, C., Li, C., Wang, B., Zhang, R., Fu, K., Gale, W.J., and Li, C. (2018). Programmed cell death in wheat (*Triticum aestivum* L.) endosperm cells is affected by drought stress. Protoplasma 255, 1039–1052.
Li, H., Liu, Y., Qin, H., Lin, X., Tang, D., Wu, Z., Luo, W., Shen, Y., Dong, F., Wang, Y., et al. (2020). A rice chloroplast-localized ABC transporter ARG1 modulates cobalt and nickel homeostasis and contributes to photosynthetic capacity. New Phytol 228, 163–178.
Liu, G., Wu, Y., Xu, M., Gao, T., Wang, P., Wang, L., Guo, T., and Kang, G. (2016a). Virus-induced gene silencing identifies an important role of the *TaRSR1* transcription factor in starch synthesis in bread wheat. Int J Mol Sci 17, 1557.
Liu, J., Cheng, X.L., Liu, P., Li, D.Y., Chen, T., Gu, X.F., and Sun, J.Q. (2017). MicroRNA319-regulated TCPs interact with FBHs and PFT1 to activate *CO* transcription and control flowering time in *Arabidopsis*. PLoS Genet 13, e1006833.
Liu, Y.C., Hou, J., Wang, X.L., Li, T., Majeed, U., Hao, C.Y., and Zhang, X.Y. (2020). The NAC transcription factor NAC019-A1 is a negative regulator of starch synthesis in wheat developing endosperm. J Exp Bot 71, 5794–5807.
Liu, Y.Y., Wang, R.L., Zhang, P., Sun, L., and Xu, J. (2016b). Involvement of reactive oxygen species in lanthanum-induced inhibition of primary root growth. J Exp Bot 67, 6149–6159.
Lu, G., Wang, X., Liu, J., Yu, K., Gao, Y., Liu, H., Wang, C., Wang, W., Wang, G., Liu, M., et al. (2014). Application of T-DNA activation tagging to identify glutamate receptor-like genes that enhance drought tolerance in plants. Plant Cell Rep 33, 617–631.
Luo, J., Li, S., Xu, J., Yan, L., Ma, Y., and Xia, L. (2021). Pyramiding favorable alleles in an elite wheat variety in one generation by CRISPR-Cas9-mediated multiplex gene editing. Mol Plant 14, 847–850.
McMaugh, S.J., Thistleton, J.L., Anschaw, E., Luo, J., Konik-Rose, C., Wang, H., Huang, M., Larroque, O., Regina, A., Jobling, S.A., et al. (2014). Suppression of starch synthase I expression affects the granule morphology and granule size and fine structure of starch in wheat endosperm. J Exp Bot 65, 2189–2201.
Mittler, R. (2017). ROS are good. Trends Plant Sci 22, 11–19.
Mittler, R., Vanderauwera, S., Gollery, M., and Van Breusegem, F. (2004). Reactive oxygen gene network of plants. Trends Plant Sci 9, 490–498.
Nayar, S., Sharma, R., Tyagi, A.K., and Kapoor, S. (2013). Functional delineation of rice *MADS29* reveals its role in embryo and endosperm development by affecting hormone homeostasis. J Exp Bot 64, 4239–4253.
Nellaepalli, S., Ozawa, S.I., Kuroda, H., and Takahashi, Y. (2018). The photosystem I assembly apparatus consisting of Ycf3-Y3IP1 and Ycf4 modules. Nat Commun 9, 2439.
Nestler, J., Liu, S., Wen, T.J., Paschold, A., Marcon, C., Tang, H.M., Li, D., Li, L., Meeley, R.B., Sakai, H., et al. (2014). *Roothairless5*, which functions in maize (*Zea mays* L.) root hair initiation and elongation encodes a monocot-specific NADPH oxidase. Plant J 79, 729–740.
Paul, P., Dhatt, B.K., Miller, M., Folsom, J.J., Wang, Z., Krassovskaya, I., Liu, K., Sandhu, J., Yu, H., Zhang, C., et al. (2020). *MADS78* and *MADS79* are essential regulators of early seed development in rice. Plant Physiol 182, 933–948.
Pei, H., Teng, W., Gao, L., Gao, H., Ren, X., Liu, Y., Jia, J., Tong, Y., Wang, Y., and Lu, Z. (2022). Low-affinity SPL binding sites contribute to subgenome expression divergence in allohexaploid wheat. Sci China Life Sci doi: 10.1007/s11427-022-2202-3.

Petrov, V., Hille, J., Mueller-Roeber, B., and Gechev, T.S. (2015). ROS-mediated abiotic stress-induced programmed cell death in plants. Front Plant Sci 6, 69.

Porter, K.J., Cao, L., Chen, Y., TerBush, A.D., Chen, C., Erickson, H.P., and Osteryoung, K.W. (2021). The *Arabidopsis thaliana* chloroplast division protein FtsZ1 counterbalances FtsZ2 filament stability *in vitro*. J Biol Chem 296, 100627.

Radchuk, V., and Borisjuk, L. (2014). Physical, metabolic and developmental functions of the seed coat. Front Plant Sci 5, 510.

Radchuk, V., Weier, D., Radchuk, R., Weschke, W., and Weber, H. (2011). Development of maternal seed tissue in barley is mediated by regulated cell expansion and cell disintegration and coordinated with endosperm growth. J Exp Bot 62, 1217–1227.

Rao, Y, Jiao, R, Wang, S, Wu, X, Ye, H, Pan, C, Li, S, Xin, D, Zhou, W, Dai, G, et al. (2021). SPL36 encodes a receptor-like protein kinase that regulates programmed cell death and defense responses in rice. Rice 14, 34.

Ray, P.D., Huang, B.W., and Tsuji, Y. (2012). Reactive oxygen species (ROS) homeostasis and redox regulation in cellular signaling. Cell Signal 24, 981–990.

Ren, D., Xie, W., Xu, Q., Hu, J., Zhu, L., Zhang, G., Zeng, D., and Qian, Q. (2022). *LSL1* controls cell death and grain production by stabilizing chloroplast in rice. Sci China Life Sci 65, 2148–2161.

Schilling, S., Kennedy, A., Pan, S., Jermiin, L.S., and Melzer, R. (2020). Genome-wide analysis of MIKC-type MADS-box genes in wheat: pervasive duplications, functional conservation and putative neofunctionalization. New Phytol 225, 511–529.

Shewry, P.R., Mitchell, R.A.C., Tosi, P., Wan, Y., Underwood, C., Lovegrove, A., Freeman, J., Toole, G.A., Mills, E.N.C., and Ward, J. L. (2012). An integrated study of grain development of wheat (cv. Hereward). J Cereal Sci 56, 21–30.

Shoesmith, J.R., Solomon, C.U., Yang, X., Wilkinson, L.G., Sheldrick, S., van Eijden, E., Couwenberg, S., Pugh, L.M., Eskan, M., Stephens, J., et al. (2021). APETALA2 functions as a temporal factor together with BLADE-ON-PETIOLE2 and MADS29 to control flower and grain development in barley. Development 148, 194894.

Song, Y., Luo, G., Shen, L., Yu, K., Yang, W., Li, X., Sun, J., Zhan, K., Cui, D., Liu, D., et al. (2020). *TubZIP28*, a novel bZIP family transcription factor from *Triticum urartu*, and *TabZIP28*, its homologue from *Triticum aestivum*, enhance starch synthesis in wheat. New Phytol 226, 1384–1398.

Usami, H., Maeda, T., Fujii, Y., Oikawa, K., Takahashi, F., Kagawa, T., Wada, M., and Kasahara, M. (2012). CHUP1 mediates actin-based light-induced chloroplast avoidance movement in the moss *Physcomitrella patens*. Planta 236, 1889–1897.

Wang, L., Leister, D., Guan, L., Zheng, Y., Schneider, K., Lehmann, M., Apel, K., and Kleine, T. (2020). The *Arabidopsis* SAFEGUARD1 suppresses singlet oxygen-induced stress responses by protecting grana margins. Proc Natl Acad Sci USA 117, 6918–6927.

Wang, Z., Shen, Y., Yang, X., Pan, Q., Ma, G., Bao, M., Zheng, B., Duanmu, D., Lin, R., Larkin, R.M., et al. (2019). Overexpression of particular MADS-box transcription factors in heat-stressed plants induces chloroplast biogenesis in petals. Plant Cell Environ 42, 1545–1560.

Wu, B., Yun, P., Zhou, H., Xia, D., Gu, Y., Li, P., Yao, J., Zhou, Z., Chen, J., Liu, R., et al. (2022). Natural variation in *WHITE-CORE RATE 1* regulates redox homeostasis in rice endosperm to affect grain quality. Plant Cell 34, 1912–1932.

Wu, J., Lawit, S.J., Weers, B., Sun, J., Mongar, N., Van Hemert, J., Melo, R., Meng, X., Rupe, M., Clapp, J., et al. (2019). Overexpression of *zmm28* increases maize grain yield in the field. Proc Natl Acad Sci USA 116, 23850–23858.

Xiao, J., Liu, B., Yao, Y., Guo, Z., Jia, H., Kong, L., Zhang, A., Ma, W., Ni, Z., Xu, S., et al. (2022). Wheat genomic study for genetic improvement of traits in China. Sci China Life Sci 65, 1718–1775.

Xu, S.B., Yu, H.T., Yan, L.F., and Wang, T. (2010). Integrated proteomic and cytological study of rice endosperms at the storage phase. J Proteome Res 9, 4906–4918.

Yang, T., Guo, L., Ji, C., Wang, H., Wang, J., Zheng, X., Xiao, Q., and Wu, Y. (2021). The B3 domain-containing transcription factor ZmABI19 coordinates expression of key factors required for maize seed development and grain filling. Plant Cell 33, 104–128.

Yang, X.L., Wu. F., Lin, X.L., Du, X.Q., Chong, K., Gramzow, L., Schilling, S., Becker, A., Theißen, G., and Meng, Z. (2012). Live and let die —the B_{sister} MADS-box gene *OsMADS29* controls the degeneration of cells in maternal tissues during seed development of rice (*Oryza sativa*). PLoS ONE 7, e51435.

Yin, L.L., and Xue, H.W. (2012). The *MADS29* transcription factor regulates the degradation of the nucellus and the nucellar projection during rice seed development. Plant Cell 24, 1049–1065.

Zhang, K., Wang, F., Liu, B., Xu, C., He, Q., Cheng, W., Zhao, X., Ding, Z., Zhang, W., Zhang, K., et al. (2021). ZmSKS13, a cupredoxin domain-containing protein, is required for maize kernel development via modulation of redox homeostasis. New Phytol 229, 2163–2178.

SUPPORTING INFORMATION

The supporting information is available online at https://doi.org/10.1007/s11427-022-2286-0. The supporting materials are published as submitted, without typesetting or editing. The responsibility for scientific accuracy and content remains entirely with the authors.